



Article

Effect of Hydrophobic Polypeptide Length on Performances of Thermo-Sensitive Hydrogels

Jiandong Han ^{1,2} , Xingyu Zhao ², Weiguo Xu ², Wei Wang ^{1,*}, Yuping Han ^{2,3,*} and Xiangru Feng ^{2,*} 

¹ Department of Chemistry, Changchun University of Science and Technology, Changchun 130022, China; jdhan@ciac.ac.cn

² Key Laboratory of Polymer Ecomaterials, Changchun Institute of Applied Chemistry, Chinese Academy of Sciences, Changchun 130022, China; star20012002@163.com (X.Z.); wgxu@ciac.ac.cn (W.X.)

³ Department of Urology, China-Japan Union Hospital of Jilin University, Changchun 130033, China

* Correspondence: weiwangl@163.com (W.W.); hyp181818@126.com (Y.H.); xrfeng@ciac.ac.cn (X.F.)

Received: 12 April 2018; Accepted: 21 April 2018; Published: 25 April 2018



Abstract: Thermosensitive gels are commonly used as drug carriers in medical fields, mainly due to their convenient processing and easy functionalization. However, their overall performance has been severely affected by their unsatisfying biocompatibility and biodegradability. To this end, we synthesized poly(L-alanine) (PLA)-based thermosensitive hydrogels with different degrees of polymerization by ring-opening polymerization. The obtained mPEG₄₅–PLA copolymers showed distinct transition temperatures and degradation abilities. It was found that slight changes in the length of hydrophobic side groups had a decisive effect on the gelation behavior of the polypeptide hydrogel. Longer hydrophobic ends led to a lower gelation temperature of gel at the same concentration, which implied better gelation capability. The hydrogels showed rapid gelling, enhanced biocompatibility, and better degradability. Therefore, this thermosensitive hydrogel is a promising material for biomedical application.

Keywords: amphiphilicity; phase change; polyamino acids; degradability

1. Introduction

The application of hydrogels in the biomedical field has rapidly increased over the past decade, including use in three-dimensional (3D) cell culture [1–3], drug delivery [4–6], and tissue engineering [7–9]. Polymer hydrogels can trap a large amount of moisture inside for easier cell membrane penetration and drug transmission. They enjoy excellent physical properties and exhibit a controllable degradation process. On account of the incomparable convenience, the in situ gelation of biodegradable hydrogels has aroused great interest in many researchers. Among numerous biodegradable hydrogels, thermosensitive hydrogels have specific advantages. On the one hand, they are rather safe for clinical utilization because the common thermosensitive gel preparation process does not involve the use of organic solvents. On the other hand, the gelling conditions of heat-sensitive hydrogels are easy to control, making them applicable in the field of biomedicine [10–12].

Thermosensitive hydrogels can be generated from block copolymers consisting of hydrophilic poly(ethylene glycol) (PEG) and hydrophobic moieties such as poly(lactic acid) (PLA) [13,14], poly(lactic-co-glycolic acid) (PLGA) [15–17], poly(ϵ -caprolactone) (PCL) [18–20], polyamidoamine (PAMAM) [21], and so on. Thermosensitive hydrogels are soluble at low temperatures, which facilitates the introduction of chemotherapeutic drugs [22–24], functional proteins [25], and cells. Due to the amorphous form of the hydrogel at low temperatures, it can be seamlessly filled into injury

sites [26,27]. At body temperature, the soluble hydrogels turn into a gel state and provide a depot for the encapsulated medical agents to achieve sustained release and long-term therapeutic effect [28]. For example, growth factors can be slowly and continuously released locally for the efficient repair of bone and nerve tissues [29–31]. The hydrogels can also function as 3D scaffolds and as a nutrient resource for cell growth in tissue engineering [32], aiming to help cells grow in a more uniform manner and promote cell proliferation [33].

In 2012, Qian's team prepared a bionic hydrogel composed of three components (i.e., triblock PEG–PCL–PEG copolymer (PECE), nano-hydroxyapatite (n-HA), and collagen), which showed satisfactory efficacy in skull repair [34]. In 2015, Chen's team engineered a thermosensitive PLGA–PEG–PLGA hydrogel loaded with 5-fluorouracil for the prevention of postoperative tendon adhesion, and acquired a good histological score [35]. However, despite the wide application of thermosensitive hydrogels in various diseases in clinical practice, they are not free from flaws. Some hydrogels are difficult to gelatinize, and the degradation time is uncontrollable. Moreover, hydrogels with poor biocompatibility always lead to severe tissue damages. Therefore, there is an urgent need to develop thermosensitive polypeptide polymers with good biocompatibility and biodegradability to avoid the above problems.

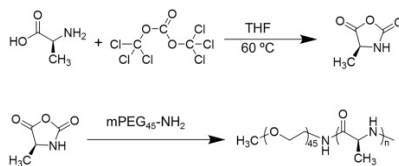
Towards this aim, peptide systems have been developed to avoid evoking the formation of an acidic microenvironment during degradation, and thus reduce the damages to surrounding tissues and minimize the adverse effects toward the bioactivity of the loaded protein or cells. Apart from this, the gelation performance of the polypeptide copolymer can be tuned by copolymerization with various hydrophobic or hydrophilic amino acid monomers, which widens the clinical applications. In 2011, Jeong's team reported the synthesis of poly(alanine-co-leucine)–poloxamer–poly(alanine-co-leucine) (PAL–PLX–PAL) hydrogels, which exhibited a sustained drug release pattern without producing evident inflammatory effects [22]. In 2017, methoxy poly(ethylene glycol)-*block*-poly(L-alanine-co-L-phenylalanine) mPEG-*b*-PLAF hydrogel was synthesized by the ring-opening polymerization (ROP) reaction of L-alanine *N*-carboxyanhydrides (L-Ala NCA) and L-phenylalanine NCA, with amino-terminated mPEG (mPEG-NH₂) as a macroinitiator. Encapsulated with combretastatin A4 (CA4) and doxorubicin (DOX), mPEG-*b*-PLAF hydrogel had an excellent inhibitory effect on the proliferation of B16F10 melanoma cells [36].

In this work, mPEG–poly(L-alanine) (mPEG–PLA_{la}) polymers with different degrees of polymerization (DPs) were synthesized and named mPEG₄₅–PLA_{la30}, mPEG₄₅–PLA_{la22}, and mPEG₄₅–PLA_{la14}. The influence of different DPs on the gelation properties of hydrogels was studied. It was found that hydrogels with higher DP showed better gelation ability than those with lower DP. In addition, the gelation behavior, tissue safety, and cytotoxicity of these polymers *in vitro* and *in vivo* were also tested and evaluated. The study revealed that these hydrogels had notable potential for employment in the biomedical field.

2. Results and Discussion

2.1. Material Synthesis and Structure Characterization

Triphosgene and L-alanine were synthesized into L-Ala NCA in dried tetrahydrofuran (THF) solvent, as shown in Scheme 1. The polypeptide hydrogels were produced via the ROP of L-Ala NCA initiated by mPEG₄₅-NH₂. The mPEG₄₅–PLA_{la} copolymers with different DPs were synthesized by altering the feed amount. The DPs of PLA_{la} were determined by contrasting the integral of the methyl peaks of side chains (–CH₃) with the methylene peak of PEG (–CH₂CH₂O–). The DPs of mPEG₄₅–PLA_{la30}, mPEG₄₅–PLA_{la22}, and mPEG₄₅–PLA_{la14} were 30, 22, and 14, respectively.



Scheme 1. Synthetic routes of L-alanine *N*-carboxyanhydrides (L-Ala NCA) and methoxy poly(ethylene glycol)–poly(L-alanine) (mPEG₄₅–PLAAla).

The typical proton nuclear magnetic resonance (¹H NMR) spectrum of block copolymer is shown in Figure 1a, and all peaks could be accurately assigned. The peaks at 1.47, 3.40, 3.50–3.80, and 4.64 ppm stood for the protons of alanine methyl, mPEG terminal methoxy, mPEG backbone, and polymer methine, respectively, indicating the successful synthesis of the three polymers.

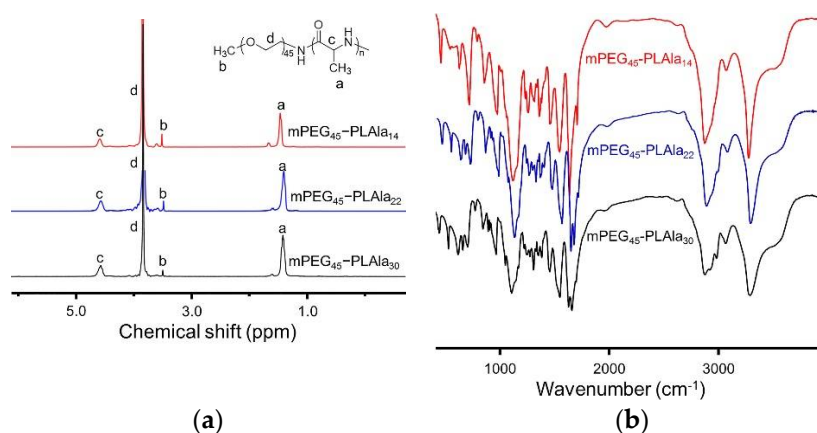


Figure 1. Structure characterization of mPEG₄₅–PLAAla. (a) ¹H NMR spectra of mPEG₄₅–PLAAla₃₀, mPEG₄₅–PLAAla₂₂, and mPEG₄₅–PLAAla₁₄, where the subscripts indicate the degree of polymerization (DP); (b) Fourier-transform infrared (FT-IR) spectra of mPEG₄₅–PLAAla₃₀, mPEG₄₅–PLAAla₂₂, and mPEG₄₅–PLAAla₁₄.

The secondary structure of the copolymer was studied by FT-IR. In Figure 1b, characteristic peaks of amide bond at 1627 cm⁻¹ and 1544 cm⁻¹ were observed, indicating that all copolymers went through the main β-sheet conformation.

2.2. Gelation Ability and Internal Appearance

The tube inversion method was used to determine the transition temperatures. Polypeptides were solubilized in a phosphate-buffered saline (PBS) solution, and went through a solution–gel transition with the change in temperature. The samples were defined as gel if they stayed still when the vial was inverted for as long as 30 s. The phase diagrams of mPEG₄₅–PLAAla₃₀ and mPEG₄₅–PLAAla₂₂ copolymers are shown in Figure 2a,b. Only copolymers with a DP of no less than 22 could undergo solution–gel transition at the concentration of 3.0–8.0 wt. %. It was noticeable that mPEG₄₅–PLAAla₂₂ showed a higher gel transition temperature than mPEG₄₅–PLAAla₃₀. The critical gelation temperatures (CGTs) of mPEG₄₅–PLAAla₃₀ and mPEG₄₅–PLAAla₂₂ were 5 °C and 15 °C, respectively, at the concentration of 5.0 wt. %. The lower CGT of mPEG₄₅–PLAAla₃₀ could be explained by longer hydrophobic end than that of mPEG₄₅–PLAAla₂₂ [37].

Solution phase behaviors of the three copolymers at different temperatures were investigated. The images in Figure 2a,b showed the mPEG₄₅–PLAAla₃₀ and mPEG₄₅–PLAAla₂₂ solutions in PBS (5.0 wt. %) at 4 °C and 37 °C. Although all copolymers were dispersed in PBS at 4 °C, the mPEG₄₅–PLAAla₁₄ formed a clear solution while mPEG₄₅–PLAAla₃₀ and mPEG₄₅–PLAAla₂₂ showed a turbid state. When temperature rose to 37 °C, mPEG₄₅–PLAAla₃₀ and mPEG₄₅–PLAAla₂₂ were

observed to be stably gelled within 5 min, while mPEG₄₅–PLA₁₄ remained in a viscous flow state. This was because mPEG₄₅–PLA₁₄ had better water solubility. Further, the morphology of the mPEG₄₅–PLA₃₀ hydrogel (5.0 wt. %) was observed by scanning electron microscope (SEM). As can be seen in Figure 2c, it was found that there were numerous tiny pores in the mPEG₄₅–PLA₃₀ gel, which was due to the 3D network structure of the gel. These pores showed a size of about 100 μm and were evenly distributed within the hydrogel, making them suitable as a depot for therapeutic agents. These findings prove that mPEG₄₅–PLA₃₀ and mPEG₄₅–PLA₂₂ hydrogels feature good stability at body temperature and are suitable for biomedical applications.

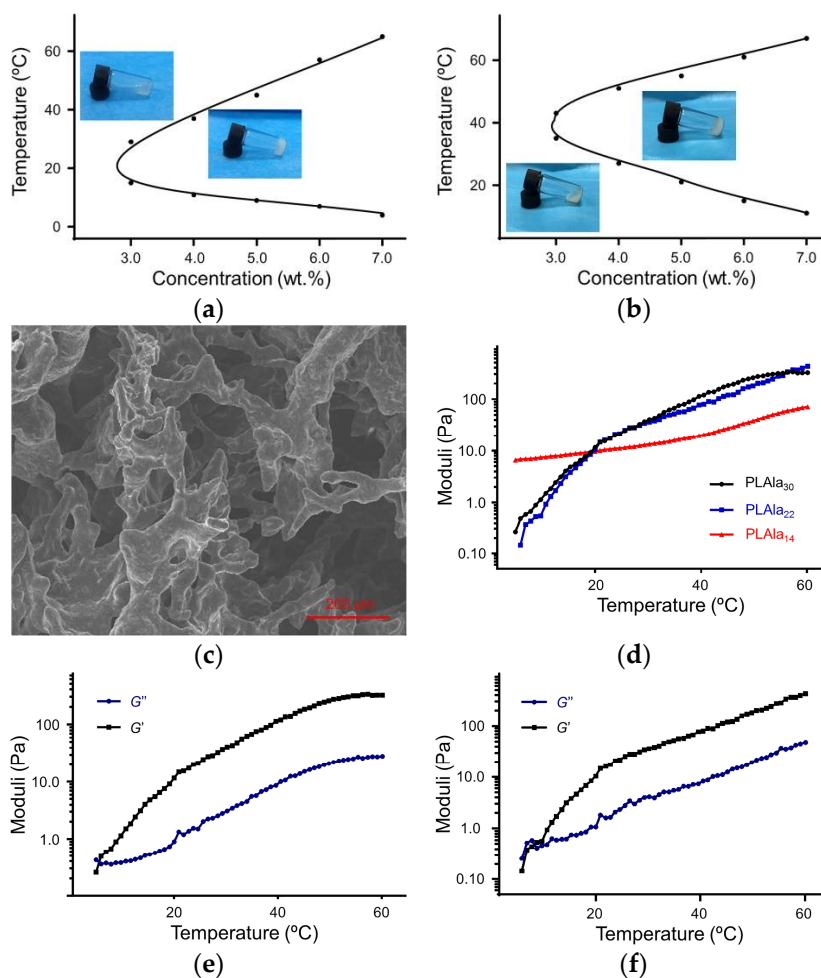


Figure 2. Gelatinization characteristics of mPEG₄₅–PLA. (a) Solution–gel phase diagrams of the mPEG₄₅–PLA₃₀ and (b) mPEG₄₅–PLA₂₂ copolymer solutions; (c) Scanning electron microscope (SEM) image of mPEG₄₅–PLA₃₀ hydrogels formed at 40 °C; (d) G' of the mPEG₄₅–PLA₃₀ (PLA₃₀), mPEG₄₅–PLA₂₂ (PLA₂₂), and mPEG₄₅–PLA₁₄ (PLA₁₄) at the concentration of 5.0 wt. % in phosphate-buffered saline (PBS) solution; (e) Changes of G' and G'' of mPEG₄₅–PLA₃₀ and (f) mPEG₄₅–PLA₂₂ in PBS solutions (5 wt. %).

2.3. Mechanical Performance Test

Thermally induced storage modulus (G') and loss modulus (G'') changes of the three copolymers were obtained by dynamic mechanical analysis. G' represents the systematic gel-like behavior of the elastic component of the complex modulus, and G'' is an index of the viscous component of the complex modulus and a measure of the sol-like behavior. The intersection of G' and G'' reflects the sol–gel transition. As shown in Figure 2d, the G' of mPEG₄₅–PLA₃₀ and mPEG₄₅–PLA₂₂ obviously increased along with rising temperatures. However, only a minor increment in G' was

seen in mPEG₄₅–PLA₁₄, and no significant change in G' was detected, even when the temperature rose to about 50 °C, implying that there was no sol–gel modification of mPEG₄₅–PLA₁₄ within the experimental temperature range. The reason was that hydrophilic mPEG was longer than the hydrophobic end made up of polypeptides. Therefore, with a longer hydrophilic segment, mPEG₄₅–PLA₁₄ showed better water solubility than mPEG₄₅–PLA₃₀ and mPEG₄₅–PLA₂₂, thus featuring less obvious sol–gel change. Notably, the length of the hydrophobic side chain had a remarkable effect on the gelation function of the mPEG–peptide block copolymer.

In Figure 2e,f, G' was smaller than G'' when the temperature was lower than CGTs (5 °C in mPEG₄₅–PLA₃₀ and 12 °C in mPEG₄₅–PLA₂₂), which reflected the viscous state of hydrogels. As the temperature increased above CGTs, G' was sharply elevated and surpassed G'' , confirming the gel formation. This result was in accordance with the findings in Figure 2a,b.

2.4. Mechanism of Gelatinization

In order to study the mechanism of sol–gel transition, the nuclear magnetic peak changes, diameter changes, and conformation evolution of polypeptides in response to temperature were tested by carbon nuclear magnetic resonance (¹³C-NMR), dynamic light scattering (DLS), and circular dichroism (CD). As shown in Figure 3a, when temperature rose from 20 to 60 °C, the characteristic peak of PEG gradually moved from 69.7 to 70.3 ppm, which revealed continuous dehydration of the PEG block during the heat-induced sol–gel transition process. Two main reasons accounted for the gelation of polymers. First, the interaction between hydrophobic blocks became stronger as temperature increased. Secondly, dehydration of PEG segments facilitated the aggregation of the hydrogels [38].

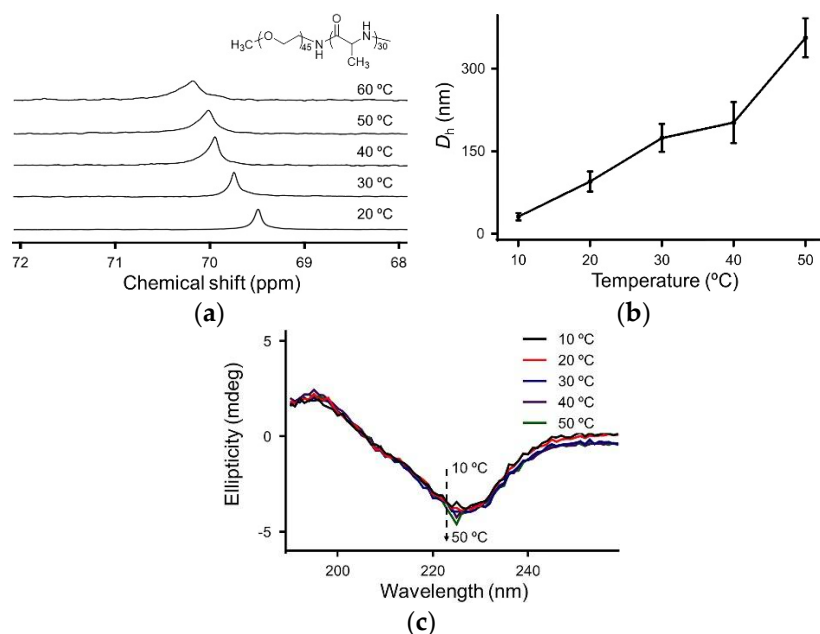


Figure 3. Gelation mechanism of the hydrogels. (a) ¹³C-NMR spectra (in D₂O) of 5.0 wt. % mPEG₄₅–PLA₃₀ solution as a function of temperature; (b) Average hydrodynamic diameter (D_h) of micelles of mPEG₄₅–PLA₃₀ as a function of temperature in water (5.0 $\mu\text{g mL}^{-1}$); (c) Circular dichroism (CD) spectra of mPEG₄₅–PLA₃₀ (0.05 mg mL^{-1}) in aqueous solution as a function of temperature.

As seen in Figure 3b, the diameter changes of mPEG₄₅–PLA₃₀ were determined at the concentration of 5.0 $\mu\text{g mL}^{-1}$. At 10 °C, the average hydrodynamic diameter (D_h) of mPEG₄₅–PLA₃₀ was about 31.4 nm. When the temperature rose to 20 °C and 50 °C, the number swiftly increased to 95.9 nm and 356.2 nm, respectively. The dramatic changes in particle size could be explained by the

interaction between the shell of PEG and core of polypeptides caused by the dehydration process of PEG [38].

In Figure 3c, the CD spectrum illustrated the alteration of the secondary structure of the aqueous mPEG₄₅–PLA₃₀ during the sol–gel transition process. The two typical bands corresponding to the β -sheet conformation, a positive Cotton band at 195 nm and a negative Cotton band at 226 nm, were clearly shown. The above results revealed that the synthesized thermosensitive hydrogel had good physicochemical properties and a clear solution–gel transformation mechanism.

2.5. Degradability Test and Pathological Analysis

Since hydrogels are often used in the biomedical field, biodegradability is a decisive factor for clinical application. If the degradation rate of the hydrogel is too high, it will lead to a rapid release of the payload. In contrast, if the hydrogel requires a long time to degrade, then it will probably remain at the injection site even after all drugs are released, which is inconvenient for further treatment. The *in vitro* degradation of mPEG₄₅–PLA₃₀ hydrogel (5.0 wt. %) was evaluated in PBS and PBS with elastase K or α -chymotrypsin. As shown in Figure 4a, there was a mass loss of over 70% and 67% hydrogel in the elastase K and α -chymotrypsin groups on day 15, respectively—considerably higher than 20% in PBS. The results could be explained by the absence of elastase K or α -chymotrypsin, where the mass loss of gels was merely attributed to the surface erosion of the hydrogels. However, with elastase K or α -chymotrypsin, the polypeptide chains of the hydrogels were also fast degrading, which sped up the loss of gels.

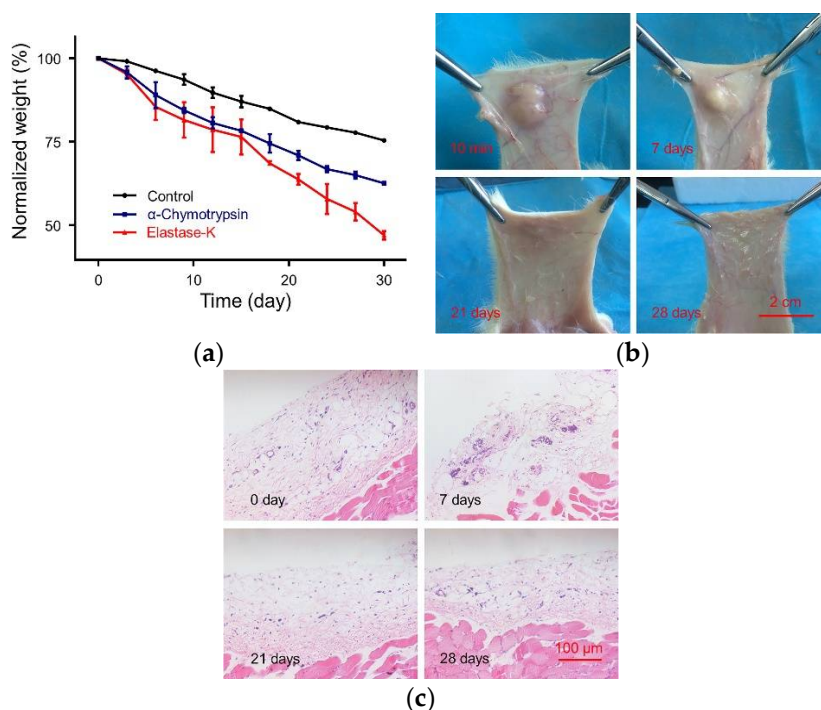


Figure 4. Degradation of hydrogel *in vitro* and *in vivo*, and histological analysis of skin. (a) Mass loss curves of *in vitro* degradation of hydrogels in PBS, and PBS with elastase-K or α -chymotrypsin (0.2 mg mL^{-1}) groups; (b) Images of *in vivo* gel maintenance at 10 min, 7, 14, 21, and 28 days after the injection of 5.0 wt. % mPEG₄₅–PLA₃₀ hydrogels; (c) Hematoxylin and eosin (H&E) images of the skin tissue near the hydrogels on day 7, 14, 21, and 28, respectively.

The degradation process of hydrogels *in vivo* was monitored for 28 days, and images were taken at 10 min, 7, 14, 21, and 28 days after hydrogel treatment. At 4°C , $500.0 \text{ }\mu\text{L}$ of mPEG₄₅–PLA₃₀ solution (5.0 wt. %) was subcutaneously injected into Sprague–Dawley (SD) rats through 21-gauge

syringe needles. In Figure 4b, the solution rapidly turned into gel in 10 min after injection. Seven days later, only a small portion of the hydrogel was degraded. On day 14, the size of the hydrogel shrank to less than 50%, while on day 28, the hydrogel was completely degraded. This degradation rate of hydrogel was suitable for application in biomedical fields requiring long-term treatment, such as tissue repair. As shown in Figure 4c, at different time intervals, the tissue surrounding the gel was surgically separated and processed by H&E staining to examine the condition of tissue damage. Basically, no histological damage or immune response was found at any time point.

2.6. Safety Evaluation

The cytotoxicity of hydrogel mPEG₄₅–PLA₃₀ in vitro was evaluated by methyl thiazolyl tetrazolium (MTT) assay and hemolysis test. In Figure 5a, L929 cells treated with the highest concentration of mPEG₄₅–PLA₃₀ (100.0 $\mu\text{g mL}^{-1}$) for 24 h retained almost 100% viability, confirming its excellent biocompatibility. Moreover, the effect of different concentrations of gel on hemolysis was also investigated. In this part, hemolysis was measured spectroscopically according to previously reported methods [39]. As shown in Figure 5b, no hemolysis was detected in blood samples treated with all test concentrations of mPEG₄₅–PLA₃₀, which further confirmed the outstanding biocompatibility. Overall, the findings above revealed that the hydrogel showed little toxicity, both in vitro and in vivo. Therefore, it is a promising material for usage in clinical practice.

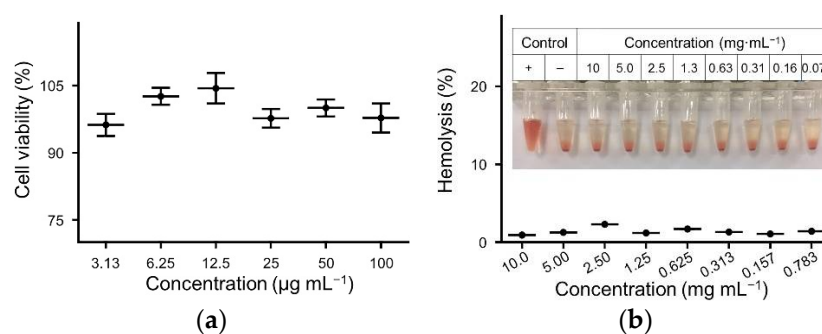


Figure 5. Biological compatibility of mPEG₄₅–PLA₃₀. (a) In vitro cytotoxicity of the mPEG₄₅–PLA₃₀ toward L929 cells. Data were presented as mean \pm SD ($n = 5$); (b) Hemolysis experiments of mPEG₄₅–PLA₃₀. Data are presented as mean \pm SD ($n = 3$).

3. Materials and Methods

3.1. Materials

mPEG–OH, number-average molecular weight (M_n) = 2000 g mol^{-1} , was purchased from Sigma-Aldrich (St. Louis, MO, USA). The mPEG₄₅–NH₂ was synthesized conforming to the previously reported protocol in our work [40]. THF and toluene were refluxed with sodium and distilled under nitrogen before usage. *N,N*-Dimethylformamide (DMF) was stored over calcium hydride (CaH₂) and purified by vacuum distillation. All the other reagents and solvents were bought from Sinopharm Chemical Reagent Co. Ltd., Beijing, China, and used as obtained.

3.2. Phase Diagram

The sol–gel transition behavior of the copolymers in PBS (pH 7.4) was determined by inverting test method with a temperature increment of 2 $^{\circ}\text{C}$ per step. Samples with concentrations ranging from 3.0–7.0 wt. % were dissolved in PBS and stirred at 0 $^{\circ}\text{C}$ for 12 h. The copolymer solution (0.2 mL) was introduced into the test tube with an inner diameter of 10.0 mm. The sol–gel transition temperature was recorded if no flow was observed within 30 s after inverting the test tube. Each data point was the average of three measurements.

3.3. Dynamic Mechanical Analysis

Rheological experiments were performed on a US 302 Rheometer (Anton Paar, Graz, Austria). The copolymer solution was placed between parallel plates of 25.0 mm in diameter with a gap of 0.5 mm. To prevent the evaporation of water, the outer edge of the sandwiched sample was sealed by a thin layer of silicon oil. The data were collected under a controlled strain γ of 1% and a frequency of 1 rad s^{-1} . The heating rate was $1 \text{ }^{\circ}\text{C min}^{-1}$.

3.4. In Vitro Gel Degradation

For this, 0.5 mL of mPEG₄₅–PLA₃₀ hydrogel was incubated in PBS (5.0 wt. %) in vials (diameter = 16.0 mm) at 37 °C for 10 min. PBS solutions (pH 7.4) containing 0.2 mg mL^{−1} elastase K or 0.2 mg mL^{−1} α -chymotrypsin were used as degradation media, and hydrogels incubated in PBS were only used as a control. Different solutions (2.0 mL) were added to the top of the gels at 37 °C and the entire medium was changed daily. The weight of the remaining gel was measured daily.

3.5. In Vivo Gel Degradation

SD rats (about 180.0 g, provided by Beijing Vital River Laboratory Animal Technology Co., Ltd., Beijing, China) were used for the detection of gel degradation in vivo. Rats were anesthetized by inhalation of ether before 0.5 mL of mPEG₄₅–PLA₃₀ PBS solutions (5.0 wt. %) were injected into the dorsal subcutaneous area of the rats using a 21-gauge needle. The rats were sacrificed on day 7, day 14, day 21, and day 28, respectively, to monitor the degradation behavior of the gel. The experiments on animals were carried out according to the guide for the care and use of laboratory animals, provided by Jilin University, Changchun, China, and the procedure was approved by the local Animal Ethics Committee.

3.6. Cytotoxicity Measurement

The relative cytotoxicity was assessed by MTT viability assay against L929 mouse fibroblasts cells. L929 cells were cultured in complete Dulbecco's modified Eagle's medium (DMEM) supplemented with 10.0% (v/v) FBS, penicillin (50.0 IU mL^{−1}), and streptomycin (50.0 IU mL^{−1}) at 37 °C in a 5.0% (v/v) carbon dioxide atmosphere. L929 cells with a density of 6000 cells per well were planted in 96-well plates in 180.0 μL of DMEM. After incubation for 24 h, 20.0 μL of copolymer solutions at different concentrations (31.3–1000.0 $\mu\text{g mL}^{-1}$) were added. L929 cells were incubated with copolymers for another 24 h before 20.0 μL of PBS solution containing MTT (0.05 mg mL^{−1}) was added and incubated for a further 4 h. Then, the media was replaced with 160.0 μL of dimethyl sulfoxide (DMSO). The absorbance of the solution was measured on a Bio-Rad 680 microplate reader (Hercules, CA, USA) at 490 nm. Cell viability (%) was calculated according to the following Equation (1).

Measurements were done in five replicates.

$$\text{Cell viability (\%)} = A_{\text{sample}} / A_{\text{control}} \times 100, \quad (1)$$

where A_{sample} and A_{control} denote the absorbances of sample and control, respectively.

4. Conclusions

In this work, thermosensitive hydrogels mPEG₄₅–PLA_n with three different DP (14, 22, and 30) were synthesized by ROP of L-Ala NCA monomer initiated by mPEG₄₅–NH₂. The effect of different DP on the solution–gel transition was investigated. It is worth noting that mPEG₄₅–PLA₃₀ had a lower sol–gel transition temperature than mPEG₄₅–PLA₂₂, attributed to the longer hydrophobic segment. In addition, mPEG–PLA_n hydrogel had good stability and high mechanical strength after gelation. Moreover, mPEG–PLA_n hydrogel did not cause any tissue damage, inflammatory reaction, or hemolysis reaction during degradation, confirming its good biocompatibility. In summary,

the mPEG–PLA hydrogel designed in our study had improved biocompatibility, appropriate degradation, and gelation ability. Therefore, the polypeptide hydrogels showed promise for application in tissue repair and regeneration, cell 3D culture, and treatment of cancer. Moreover, by loading functional drugs, the hydrogels can also be used for postoperative recovery and anti-infection. Based on the above findings, polypeptide thermosensitive hydrogels have broad prospects in the biomedical field.

Supplementary Materials: The following are available online.

Author Contributions: W.X. and W.W. conceived and designed the experiments; J.H. performed the experiments; J.H., X.Z. and X.F. analyzed the data; and Y.H. contributed reagents and materials. J.H. initiated and wrote this article; X.F. helped to write and corrected the manuscript; and Y.H. discussed and suggested ideas for improvement of this article.

Acknowledgments: This research was supported by the Key Technology Research and Development Project of Jilin Department of Science and Technology (No. 20180201083GX) and Natural Science Foundation of Jilin Department of Science and Technology (20170101107JC).

Conflicts of Interest: The authors declare no conflict of interest.

References

1. Ravi, M.; Paramesh, V.; Kaviya, S.R.; Anuradha, E.; Solomon, F.D. 3D cell culture systems: Advantages and applications. *J. Cell Physiol.* **2015**, *230*, 16–26. [[CrossRef](#)] [[PubMed](#)]
2. Tibbitt, M.W.; Anseth, K.S. Hydrogels as extracellular matrix mimics for 3D cell culture. *Biotechnol. Bioeng.* **2009**, *103*, 655–663. [[CrossRef](#)] [[PubMed](#)]
3. Zhao, T.; Sellers, D.L.; Cheng, Y.; Horner, P.J.; Pun, S.H. Tunable, injectable hydrogels based on peptide-cross-linked, cyclized polymer nanoparticles for neural progenitor cell delivery. *Biomacromolecules* **2017**, *18*, 2723–2731. [[CrossRef](#)] [[PubMed](#)]
4. Lock, L.L.; Lo, Y.; Mao, X.; Chen, H.; Staedtke, V.; Bai, R.; Ma, W.; Lin, R.; Li, Y.; Liu, G.; et al. One-component supramolecular filament hydrogels as theranostic label-free magnetic resonance imaging agents. *ACS Nano* **2017**, *11*, 797–805. [[CrossRef](#)] [[PubMed](#)]
5. Deng, Y.; Yang, F.; Cocco, E.; Song, E.; Zhang, J.W.; Cui, J.J.; Mohideen, M.; Bellone, S.; Santin, A.D.; Saltzman, W.M. Improved i.P. Drug delivery with bioadhesive nanoparticles. *Proc. Natl. Acad. Sci. USA* **2016**, *113*, 11453–11458. [[CrossRef](#)] [[PubMed](#)]
6. Zhu, M.; Wei, K.; Lin, S.; Chen, X.; Wu, C.-C.; Li, G.; Bian, L. Bioadhesive polymersome for localized and sustained drug delivery at pathological sites with harsh enzymatic and fluidic environment via supramolecular host-guest complexation. *Small* **2018**, *14*. [[CrossRef](#)] [[PubMed](#)]
7. Qu, Y.; Wang, B.; Chu, B.; Liu, C.; Rong, X.; Chen, H.; Peng, J.; Qian, Z. Injectable and thermosensitive hydrogel and pdlla electrospun nanofiber membrane composites for guided spinal fusion. *ACS Appl. Mater. Interfaces* **2018**, *10*, 4462–4470. [[CrossRef](#)] [[PubMed](#)]
8. Zhu, C.; Lei, H.; Fan, D.; Duan, Z.; Li, X.; Li, Y.; Cao, J.; Wang, S.; Yu, Y. Novel enzymatic crosslinked hydrogels that mimic extracellular matrix for skin wound healing. *J. Mater. Sci.* **2018**, *53*, 5909–5928. [[CrossRef](#)]
9. Shahriari, D.; Shibayama, M.; Lynam, D.A.; Wolf, K.J.; Kubota, G.; Koffler, J.Y.; Tuszynski, M.H.; Campana, W.M.; Sakamoto, J.S. Peripheral nerve growth within a hydrogel microchannel scaffold supported by a kink-resistant conduit. *J. Biomed. Mater. Res. Part A* **2017**, *105*, 3392–3399. [[CrossRef](#)] [[PubMed](#)]
10. Xu, H.-L.; Tian, F.-R.; Lu, C.-T.; Xu, J.; Fan, Z.-L.; Yang, J.-J.; Chen, P.-P.; Huang, Y.-D.; Xiao, J.; Zhao, Y.-Z. Thermo-sensitive hydrogels combined with decellularised matrix deliver bfgf for the functional recovery of rats after a spinal cord injury. *Sci. Rep.* **2016**, *6*, 38332. [[CrossRef](#)] [[PubMed](#)]
11. Lu, D.; Li, Y.; Li, T.; Zhang, Y.; Dou, F.; Wang, X.; Zhao, X.; Ma, H.; Guan, X.; Wei, Q.; et al. Surgical adhesive: Synthesis and properties of thermoresponsive pluronic l-31-3,4-dihydroxyphenylalanine-arginine derivatives. *J. Appl. Polym. Sci.* **2017**, *134*. [[CrossRef](#)]
12. Li, P.; Zhang, J.; Dong, C.-M. Photosensitive poly(*o*-nitrobenzyloxycarbonyl-L-lysine)-*b*-peo polypeptide copolymers: Synthesis, multiple self-assembly behaviors, and the photo/ph-thermo-sensitive hydrogels. *Polym. Chem.* **2017**, *8*, 7033–7043. [[CrossRef](#)]

13. Cui, H.; Shao, J.; Wang, Y.; Zhang, P.; Chen, X.; Wei, Y. PLA-PEG-PLA and its electroactive tetraaniline copolymer as multi-interactive injectable hydrogels for tissue engineering. *Biomacromolecules* **2013**, *14*, 1904–1912. [[CrossRef](#)] [[PubMed](#)]
14. Wang, D.K.; Varanasi, S.; Strounina, E.; Hill, D.J.T.; Symons, A.L.; Whittaker, A.K.; Rasoul, F. Synthesis and characterization of a POSS-PEG macromonomer and POSS-PEG-PLA hydrogels for periodontal applications. *Biomacromolecules* **2014**, *15*, 666–679. [[CrossRef](#)] [[PubMed](#)]
15. Michlovská, L.; Vojtova, L.; Humpa, O.; Kucerik, J.; Zidek, J.; Jancar, J. Hydrolytic stability of end-linked hydrogels from PLGA-PEG-PLGA macromonomers terminated by alpha,omega-itaconyl groups. *RSC Adv.* **2016**, *6*, 16808–16816. [[CrossRef](#)]
16. Wang, P.; Chu, W.; Zhuo, X.; Zhang, Y.; Gou, J.; Ren, T.; He, H.; Yin, T.; Tang, X. Modified PLGA-PEG-PLGA thermosensitive hydrogels with suitable thermosensitivity and properties for use in a drug delivery system. *J. Mater. Chem. B* **2017**, *5*, 1551–1565. [[CrossRef](#)]
17. Zhang, Y.; Zhang, J.; Chang, F.; Xu, W.; Ding, J. Repair of full-thickness articular cartilage defect using stem cell-encapsulated thermogel. *Mater. Sci. Eng. C* **2018**, *88*, 79–87. [[CrossRef](#)] [[PubMed](#)]
18. Dong, X.; Chen, H.; Qin, J.; Wei, C.; Liang, J.; Liu, T.; Kong, D.; Lv, F. Thermosensitive porphyrin-incorporated hydrogel with four-arm peg-pcl copolymer (ii): Doxorubicin loaded hydrogel as a dual fluorescent drug delivery system for simultaneous imaging tracking in vivo. *Drug. Deliv.* **2017**, *24*, 641–650. [[CrossRef](#)] [[PubMed](#)]
19. Luo, Z.; Jin, L.; Xu, L.; Zhang, Z.L.; Yu, J.; Shi, S.; Li, X.; Chen, H. Thermosensitive PEG-PCL-PEG (PECE) hydrogel as an in situ gelling system for ocular drug delivery of diclofenac sodium. *Drug. Deliv.* **2016**, *23*, 63–68. [[CrossRef](#)] [[PubMed](#)]
20. Wang, S.-J.; Zhang, Z.-Z.; Jiang, D.; Qi, Y.-S.; Wang, H.-J.; Zhang, J.-Y.; Ding, J.-X.; Yu, J.-K. Thermogel-coated poly(epsilon-caprolactone) composite scaffold for enhanced cartilage tissue engineering. *Polymers* **2016**, *8*, 200. [[CrossRef](#)]
21. Navath, R.S.; Menjoge, A.R.; Dai, H.; Romero, R.; Kannan, S.; Kannan, R.M. Injectable PAMAM dendrimer-PEG hydrogels for the treatment of genital infections: Formulation and in vitro and in vivo evaluation. *Mol. Pharm.* **2011**, *8*, 1209–1223. [[CrossRef](#)] [[PubMed](#)]
22. Moon, H.J.; Choi, B.G.; Park, M.H.; Joo, M.K.; Jeong, B. Enzymatically degradable thermogelling poly(alanine-co-leucine)-poloxamer-poly(alanine-co-leucine). *Biomacromolecules* **2011**, *12*, 1234–1242. [[CrossRef](#)] [[PubMed](#)]
23. Zheng, Y.; Cheng, Y.; Chen, J.; Ding, J.; Li, M.; Li, C.; Wang, J.-C.; Chen, X. Injectable hydrogel-microsphere construct with sequential degradation for locally synergistic chemotherapy. *ACS Appl. Mater. Interfaces* **2017**, *9*, 3487–3496. [[CrossRef](#)] [[PubMed](#)]
24. Cheng, Y.; He, C.; Ding, J.; Xiao, C.; Zhuang, X.; Chen, X. Thermosensitive hydrogels based on polypeptides for localized and sustained delivery of anticancer drugs. *Biomaterials* **2013**, *34*, 10338–10347. [[CrossRef](#)] [[PubMed](#)]
25. Conde, J.; Oliva, N.; Atilano, M.; Song, H.S.; Artzi, N. Self-assembled RNA-triple-helix hydrogel scaffold for microRNA modulation in the tumour microenvironment. *Nat. Mater.* **2016**, *15*, 353. [[CrossRef](#)] [[PubMed](#)]
26. Li, X.; Ding, J.; Zhang, Z.; Yang, M.; Yu, J.; Wang, J.; Chang, F.; Chen, X. Kartogenin-incorporated thermogel supports stem cells for significant cartilage regeneration. *ACS Appl. Mater. Interfaces* **2016**, *8*, 5148–5159. [[CrossRef](#)] [[PubMed](#)]
27. Zhang, Y.; Ding, J.; Sun, D.; Sun, H.; Zhuang, X.; Chang, F.; Wang, J.; Chen, X. Thermogel-mediated sustained drug delivery for in situ malignancy chemotherapy. *Mater. Sci. Eng. C* **2015**, *49*, 262–268. [[CrossRef](#)] [[PubMed](#)]
28. Zhang, Y.-B.; Ding, J.-X.; Xu, W.-G.; Wu, J.; Chang, F.; Zhuang, X.-L.; Chen, X.-S.; Wang, J.-C. Biodegradable thermogel as culture matrix of bone marrow mesenchymal stem cells for potential cartilage tissue engineering. *Chin. J. Polym. Sci.* **2014**, *32*, 1590–1601. [[CrossRef](#)]
29. Sitoci-Ficici, K.H.; Matyash, M.; Uckermann, O.; Galli, R.; Leipnitz, E.; Later, R.; Ikonomidou, C.; Gelinsky, M.; Schackert, G.; Kirsch, M. Non-functionalized soft alginate hydrogel promotes locomotor recovery after spinal cord injury in a rat hemimyelonection model. *Acta Neurochir.* **2018**, *160*, 449–457. [[CrossRef](#)] [[PubMed](#)]
30. Ansari, S.; Diniz, I.M.; Chen, C.; Sarrion, P.; Tamayol, A.; Wu, B.M.; Moshaverinia, A. Human periodontal ligament- and gingiva-derived mesenchymal stem cells promote nerve regeneration when encapsulated in alginate/hyaluronic acid 3D scaffold. *Adv. Healthc. Mater.* **2017**, *6*. [[CrossRef](#)] [[PubMed](#)]

31. Liu, H.; Ding, J.; Li, C.; Wang, C.; Wang, Y.; Wang, J.; Chang, F. Hydrogel is superior to fibrin gel as matrix of stem cells in alleviating antigen-induced arthritis. *Polymers* **2016**, *8*, 182. [[CrossRef](#)]
32. Chaudhuri, O.; Gu, L.; Klumpers, D.; Darnell, M.; Bencherif, S.A.; Weaver, J.C.; Huebsch, N.; Lee, H.-P.; Lippens, E.; Duda, G.N.; et al. Hydrogels with tunable stress relaxation regulate stem cell fate and activity. *Nat. Mater.* **2016**, *15*, 326. [[CrossRef](#)] [[PubMed](#)]
33. Knight, E.; Przyborski, S. Advances in 3D cell culture technologies enabling tissue-like structures to be created in vitro. *J. Anat.* **2015**, *227*, 746–756. [[CrossRef](#)] [[PubMed](#)]
34. Fu, S.; Ni, P.; Wang, B.; Chu, B.; Zheng, L.; Luo, F.; Luo, J.; Qian, Z. Injectable and thermo-sensitive PEG-PCL-PEG copolymer/collagen/n-ha hydrogel composite for guided bone regeneration. *Biomaterials* **2012**, *33*, 4801–4809. [[CrossRef](#)] [[PubMed](#)]
35. Yuan, B.; He, C.; Dong, X.; Wang, J.; Gao, Z.; Wang, Q.; Tian, H.; Chen, X. 5-fluorouracil loaded thermosensitive PLGA-PEG-PLGA hydrogels for the prevention of postoperative tendon adhesion. *RSC Adv.* **2015**, *5*, 25295–25303. [[CrossRef](#)]
36. Wei, L.; Chen, J.; Zhao, S.; Ding, J.; Chen, X. Thermo-sensitive polypeptide hydrogel for locally sequential delivery of two-pronged antitumor drugs. *Acta Biomater.* **2017**, *58*, 44–53. [[CrossRef](#)] [[PubMed](#)]
37. Choi, Y.Y.; Jang, J.H.; Park, M.H.; Choi, B.G.; Chi, B.; Jeong, B. Block length affects secondary structure, nanoassembly and thermosensitivity of poly(ethylene glycol)-poly(L-alanine) block copolymers. *J. Mater. Chem.* **2010**, *20*, 3416–3421. [[CrossRef](#)]
38. Cheng, Y.; He, C.; Xiao, C.; Ding, J.; Zhuang, X.; Huang, Y.; Chen, X. Decisive role of hydrophobic side groups of polypeptides in thermosensitive gelation. *Biomacromolecules* **2012**, *13*, 2053–2059. [[CrossRef](#)] [[PubMed](#)]
39. Xu, W.; Ding, J.; Xiao, C.; Li, L.; Zhuang, X.; Chen, X. Versatile preparation of intracellular-acidity-sensitive oxime-linked polysaccharide-doxorubicin conjugate for malignancy therapeutic. *Biomaterials* **2015**, *54*, 72–86. [[CrossRef](#)] [[PubMed](#)]
40. Ding, J.; Shi, F.; Xiao, C.; Lin, L.; Chen, L.; He, C.; Zhuang, X.; Chen, X. One-step preparation of reduction-responsive poly(ethylene glycol)-poly(amino acid)s nanogels as efficient intracellular drug delivery platforms. *Polym. Chem.* **2011**, *2*, 2857–2864. [[CrossRef](#)]

Sample Availability: Samples of the compounds are available from the authors.



© 2018 by the authors. Licensee MDPI, Basel, Switzerland. This article is an open access article distributed under the terms and conditions of the Creative Commons Attribution (CC BY) license (<http://creativecommons.org/licenses/by/4.0/>).